Simultaneous tracking of ultrafast surface and gas-phase dynamics in solid-gas interfacial reactions

Keith Blackman[1*], Eric Segrest[1*], George Turner[1], Kai Machamer[1], Aakash Gupta[1], Md Afjal Khan Pathan[1], S. Novia Berriel[2], Parag Banerjee[2,3,4,5], and Mihai E. Vaida[1,5a)]

[1] *Department of Physics, University of Central Florida, Orlando, Florida 32816, United States*
[2] *Department of Material Science and Engineering, University of Central Florida, Orlando, Florida 32816, United States*
[3]*Nano Science and Technology Center, University of Central Florida, Orlando, FL 32816, USA.*
[4]*Florida Solar Energy Center, University of Central Florida, Orlando, FL 32816, USA.*
[5]*Renewable Energy and Chemical Transformations Cluster, University of Central Florida, Orlando, Florida 32816, United States*

ABSTRACT

Real-time detection of intermediate species and final products at the surface and near-surface in interfacial solid-gas reactions is critical for an accurate understanding of heterogeneous reaction mechanisms. In this contribution, an experimental method that can simultaneously monitor the ultrafast dynamics at the surface and above the surface in photoinduced heterogeneous reactions is presented. The method relies on a combination of mass spectrometry and femtosecond pump-probe spectroscopy. As a model system, the photoinduced reaction of methyl iodide on and above a cerium oxide surface is investigated. The species that are simultaneously detected from the surface and gas-phase present distinct features in the mass spectra, such as a sharp peak followed by an adjacent broad shoulder. The sharp peak is attributed to the species detected from the surface while the broad shoulder is due to the detection of gas-phase species above the surface, as confirmed by multiple experiments. By monitoring the evolution of the sharp peak and broad shoulder as a function of the pump-probe time delay, transient signals are obtained that describe the ultrafast photoinduced reaction dynamics of methyl iodide on the surface and in gas-phase. Finally, SimION simulations are performed to confirm the origin of the ions produced on the surface and gas-phase.

I. INTRODUCTION

Understanding the mechanism of heterogeneous reactions at the solid-gas interface is crucial to perceive many reactions occurring in nature as well as to understand, control, and improve various chemical processes that have a high technological and industrial significance. For example, heterogeneous catalytic reactions at the solid-gas interface are responsible for about 90% of chemical production processes and more than 20% of all industrial products.[1 and Refs. therein)]

Efforts to decipher heterogeneous catalytic process have begun decades ago, employing *model catalysis,* which provides a good understanding of various elementary steps of the surface reaction on well-defined and characterized model catalyst samples under ultra-high vacuum (UHV) conditions.[2] To address the "pressure gap" between the UHV model catalysis investigations and the high pressure involved in industrial heterogeneous reactions, operando techniques have been developed, which characterize simultaneously the properties of the catalyst surface and the surface chemistry at pressures closer to those involved in real applications.[3-6] Recent efforts have also been made to develop techniques to monitor and understand the role of the gas-phase chemistry above a solid catalyst,[7] because in some solid-gas heterogeneous reactions that operate at pressures relevant for practical applications, reactive intermediate species formed on the catalyst surface could escape to the gas-phase, or be re-adsorbed at a different location on the catalyst surface.[ref. 7 and refs. therein)] These intermediates can further react in the gas phase or on the surface and consequently influence the overall reaction outcome. Therefore, experimental methods that can track in real-time the dynamics of highly unstable intermediate species and final products simultaneously

* These authors contributed equally
a) Author to whom correspondence should be addressed. E-mail: mihai.vaida@ucf.edu

at the surface and near-surface, i.e. nanometers to millimeters in the gas-phase above the surface, can be revolutionary in understanding complex heterogeneous reactions at solid-gas interfaces.

An experimental technique based on mass spectrometry in conjunction with femtosecond pump-probe spectroscopy that was introduced more than three decades ago,[8] is currently still used in many laboratories to track the ultrafast molecular dynamics in gas-phase. This technique was subsequently adapted to track the ultrafast dynamics of intermediate species and final products in photoinduced reactions on solid surfaces.[9]

In this work, an experimental technique is presented that can simultaneously monitor the ultrafast molecular dynamics at the surface and in gas-phase near-surface in photoinduced heterogeneous reactions at solid-gas interfaces. The technique relies on a combination of mass spectrometry and femtosecond pump-probe spectroscopy. To test the versatility of this technique, the photoinduced reaction dynamics of methyl iodide on a cerium oxide surface is investigated. The methyl iodide molecule is selected as a model system for photoinduced interfacial reactions, because its gas-phase photodissociation has been studied both experimentally[10-16] and theoretically.[17-24] Furthermore, the photoinduced reaction dynamics of methyl iodide has been investigated with femtosecond resolution in gas-phase[25-29] as well as on insulating,[30-32] metallic,[33] and semiconducting[34] surface. The photoinduced reaction dynamics of methyl iodide was also investigated with time, mass, and energy resolution on cerium oxide films like those used in this investigation, providing a base of comparison of the current and previously reported results.[34]

In this work, a detailed account of experimental setup employed to monitor photoinduced reactions at the gas-solid interface is provided. The ultrafast molecular dynamics experiments are performed using deuterated methyl iodide (CD_3I) dosed on a cerium oxide surface. Additional experiments in which methyl iodide (CH_3I) is dosed on insulating, semiconducting, and metal surfaces are performed to confirm the origin of the ions, i.e. surface vs gas-phase, and to estimate the local pressure near-surface. The exact type of molecule used in each experiment is mentioned in text and on each figure. SimION simulations are performed to confirm the origin of the ions produced on the surface and gas-phase.

II. EXPERIMENTAL METHODS

A. Experimental Setup

The experimental setup consists of an UHV surface science chamber equipped with various tools for surface preparation and characterization, as well as a femtosecond laser system. Details about the surface science chamber and the laser system are presented in the Supplementary Material.

B. Time-of-flight mass spectrometer

To investigate the ultrafast molecular dynamics at the solid-gas interface and distinguish between the reactions that occur at the solid surface and in gas-phase, a home built Wiley/McLaren-type time-of-flight mass spectrometer[35] (TOF-MS) is employed together with a continuous gas admission system. Except a few electrodes, which are in-house machined, the ion optics of the TOF spectrometer is constructed using "eV Parts" from Kimball Physics Inc., i.e., stainless steel plates, stainless steel cylinders, alumina spacers, alumina tubes, stainless steel compression lock rings, etc. Figure 1(a) displays a schematic cross-sectional view in the longitudinal-vertical plane of the TOF-MS head in which details on the spectrometer construction, surface, and gas tube positions are provided. A schematic representation of the whole TOF-MS is displayed in Figure S1 in the Supplementary Material. Figure 1(b) displays a cross-sectional view in the longitudinal-horizontal plane of a three-dimensional (3D) SimION simulation[36] of the ion trajectories through the TOF-MS ion optics after their formation on the laser path on the surface and near-surface.

The surface, which represents the repeller electrode of the TOF-MS is grounded and positioned perpendicular to the longitudinal spectrometer axis at 8 mm from the entrance electrode (E_1 in Figure 1). Gas-phase molecules are continuously dosed with a gas tube that has an internal diameter of 4.6 mm and ends at 12 mm from the sample surface (cf. Figure 1(a)). The pump and probe laser beams collinearly irradiate the surface at an incidence angle of about 45°. Positive ions formed on the laser path, on the surface, and above the surface are accelerated into the spectrometer by a static electric field, i.e., the first

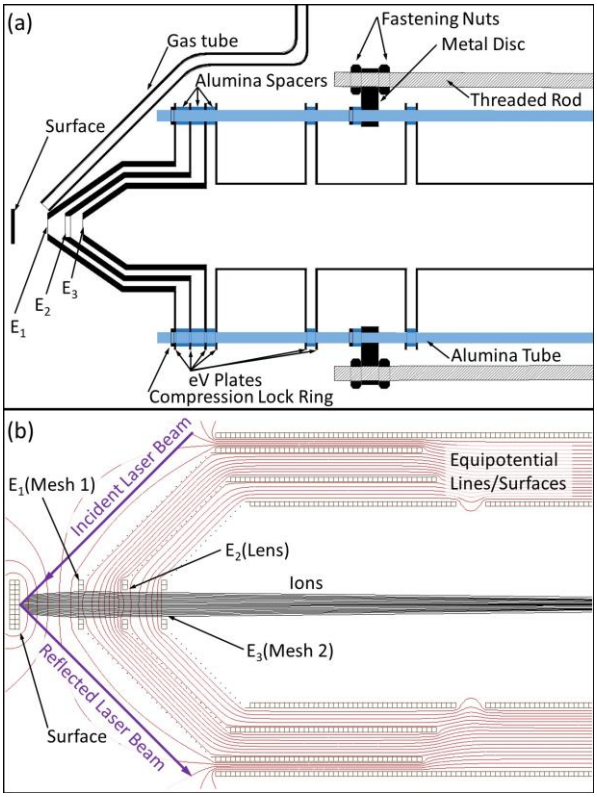

Figure 1 *(a) Schematic cross-sectional view in the longitudinal-vertical plane of the TOF-MS head, display details on the TOF construction, and the position of the surface and gas tube. (b) Cross-sectional view in the longitudinal-horizontal plane of a 3D SimION simulation of the TOF-MS displaying the incident and reflect ion beams, ion trajectories (black curves) and equipotential surfaces (red curves).*

C. Characterization of the local pressure near-surface

Temperature programmed desorption (TPD) is employed to estimate the local pressure in front of the surface at the location in which the surface is positioned when pump-probe molecular dynamics investigations are performed using the TOF-MS. TPD is a technique that is routinely employed in our laboratory to investigate the interaction between adsorbed molecules and the surface.[34, 37, 38]

First, a series of TPD spectra are recorded from a Si(111) surface on which CH_3I molecules are dosed with the gas tube while the surface sample is positioned close to the ion gauge detector, which is far from the gas tube so that the pressure can be accurately measured in the vicinity of the surface. Figure 2. acceleration region of the TOF-MS, formed between the grounded surface and the spectrometer entrance electrode (E_1 in Figure 1) on which -600 V is applied. A potential of -2000 V is applied on electrode E_3 (cf. Figure 1), to create the second acceleration region of the spectrometer. Both E_1 and E_3 electrodes are circular holes with a diameter of 3 mm on which Ni meshes with a transparency of 90% are attached. An electrostatic lens, (E_2 in Figure 1) is positioned between electrodes E_1 and E_3 to collimate ions and hence to increase the intensity of the detected ion signal. The electrode E_3 also represents the entrance in the free field region of the TOF. An einzel lens that can slightly increase the transmission of the TOF-MS (by up to 5%) by collimating the ion beam is also built into the free field region of the spectrometer. In this study, all einzel lens elements as well as the field-free drift tube are kept at -2000 V and therefore, they do not influence the trajectory or time-of-flight of positive ions. The total length of the TOF-MS field-free region is 700 mm. The ions pass the field-free region with different velocities according to their mass-to-charge ratio and are subsequently detected by a microchannel plate amplifier detector arrangement as a function of their time-of-flight. The signal acquisition is carried out by a 10 GHz multichannel scaler electronics (FAST ComTec, MCS6A).

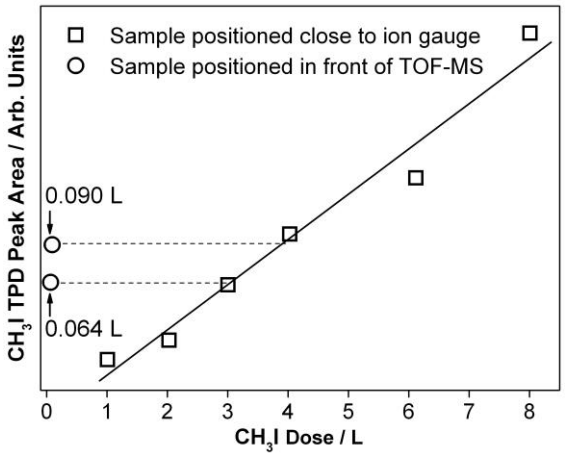

Figure 2. *Area of the CH_3I TPD signal as a function of exposure of a Si(111) surface with CH_3I gas close to the ion gauge (squares) and in front of the TOF-MS (circles). The black straight line is a linear fit of the data points taken close to the ion gauge.*

displays the surface areas of the CH_3I signal desorbed from the surface as a function of CH_3I exposure in units of Langmuir (1L=1s × 1×10^{-6} Torr). As can be seen in Figure 2, the area of the CH_3I signal increases linearly with the CH_3I exposure. Second, two TPD spectra are recorded after dosing the Si(111) surface with CH_3I molecules in front of the TOF-MS at the exact position used during pump-probe molecular dynamics investigations (cf. Figure 2). Finally, to find the local pressure in front of the TOF-MS, the CH_3I exposures that lead to the same desorption area for the two sample positions are compared. The area of the TPD peaks obtained after dosing the Si(111) surface with CH_3I molecules in front of the TOF-MS roughly corresponds to the area obtained by exposing the surface to a 45 times higher dose close to the ion gauge detector. Therefore, the local pressure in front of the surface during pump-probe molecular dynamics investigations performed with the TOF-MS is estimated to be 45 times higher than the pressure measured with the ion gauge detector.

III. PHOTOINDUCED REACTIONS AT THE GAS-SOLID INTERFACES

A. Ultrafast photoinduced reaction dynamics

As mentioned above, a model system consisting of methyl iodide or deuterated methyl iodide molecules and an amorphous cerium oxide surface is employed to investigate the ultrafast molecular dynamics at the solid-gas interface and distinguish between the reactions that occur at the solid surface and in the gas-phase near-surface. Details about the preparation and characterization of the cerium oxide surface are presented in the Supplementary Material. Methyl iodide molecules are continuously dosed with the gas tube onto the cerium oxide surface. The pump laser pulse (266 nm, 25 mW/cm^2, p-polarized) excites the methyl iodide molecules into the dissociative A-band, which leads to the formation of methyl and iodine neutral fragments. Subsequently, the probe laser pulse (266 nm, 300 mW/cm^2, p-polarized) is used to ionize the neutral fragments and reaction products that are formed on the laser path, on the surface and above the surface.

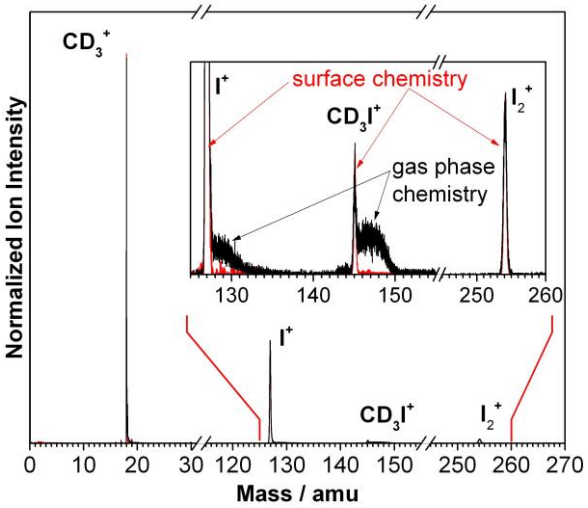

Figure 3. *Time-of-flight mass spectra obtained from CD_3I continuously dosed at a partial pressure of 5×10^{-9} Torr (red curve) and 4×10^{-8} Torr (black curve) on a 3.6 nm thin cerium oxide film grown on Si(100) at a pump-probe time delay of 4 ps. The surface is kept at 160 K during the measurement to restrict the number of molecules at the surface. Inset: Magnified view of the 125-260 amu spectral region. The spectra are obtained by summing the mass signals over 1 × 10^6 laser shots.*

Figure 3 displays mass spectra recorded from CD_3I continuously dosed on a 3.6 nm thin cerium oxide film grown on Si(100) at 5×10^{-9} Torr and 4×10^{-8} Torr. The CD_3I partial pressure is measured with an ion-gauge detector placed far from the sample and inlet gas tube. For the mass spectra displayed in Figure 3, to restrict the amount of CD_3I molecules on the surface at sub-monolayer (ML) coverage and maintain this coverage constant during the surface reaction, the cerium oxide sample temperature is kept at 160 K as demonstrated in one of our recent publications.[34] The mass spectra in Figure 3 display four peaks corresponding to CD_3^+, I^+, I_2^+, and CD_3I^+. The CD_3^+, I^+, and CD_3I^+ appear as narrow peaks when CD_3I is dosed at pressures below 5×10^{-9} Torr. When the CD_3I pressure is increased to 4×10^{-8} Torr, low intensity, broad shoulders appear after the CD_3^+, I^+, and CD_3I^+ narrow peaks (cf. insert in Figure 3). Interestingly, the I_2^+mass peak is narrow and does not present a shoulder dependent on the CD_3I gas-phase pressure. The sharp peaks resemble the mass spectra obtained from surface chemical reactions reported in our previous publications in which molecules are dosed with a pulsed valve that is synchronized with a laser shutter, which stops the laser irradiation while molecules are dosed to avoid the detection of species from gas-phase,[9, 30, 31, 33, 39, 40] or when molecules are

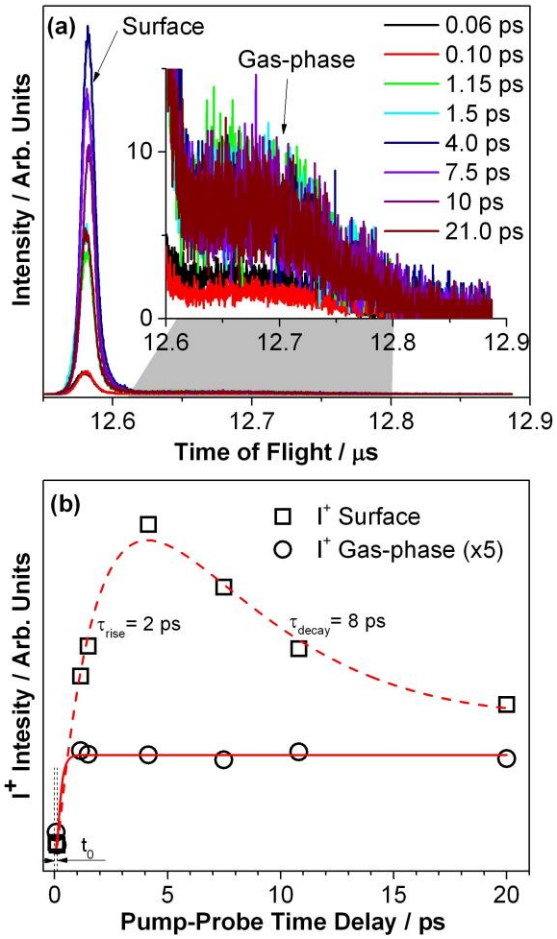

Figure 4. *(a) Mass spectra recorded at various pump-probe time delays in the 12.55-12.9 μs time-of-flight range corresponding to I^+. The insert in (a) shows a magnified view of the 12.6-12.9 μs time-of-flight range corresponding to the I^+ broad shoulder originating from the gas phase. The spectra are obtained by summing the mass signals over 2 × 10^5 laser shots. (b) Surface area of the sharp peak (black squares) and broad shoulder (red circles) as a function of the pump-probe time delay. The red curves are simulations of the measured data (see text for details).*

continuously dosed using a leak valve that maintains a low gas-phase pressure during pump-probe surface molecular dynamics investigations.[34] Several factors suggest that the broad shoulders originate from gas-phase reactions: (i) the broad shoulders of CD_3^+, I^+, and CD_3I^+ are only visible when the CD_3I gas-phase pressure is increased, which enhances the probability of detecting ions originating from the gas-phase; (ii) I_2^+ signal appears only as a sharp peak in the mass spectra independent of the CD_3I gas-phase pressure. This indicates that I_2 is only formed at the surface, because bimolecular reactions are not possible in the gas-phase at the pressures employed in this experiment, due to (a) the low density of I atoms in the gas-phase, which leads to a low probability of collisions between I atoms above the surface and hence a low probability of a bimolecular reaction in the gas-phase, and (b) low density of gas-phase molecules, which reduce the possibility of I atoms produced in the gas-phase to lose their excess translational energy released through the photodissociation process, and hence a low probability of I atoms that collide to form stable bonds in the gas-phase. As demonstrated in one of our recent publications,[34] I atoms produced via A-band photodissociation of methyl iodide at the surface are highly energetic and require multiple collisions with the surface and adjacent molecules to get thermalized to form I_2 [31, 34]. (iii) The intensity of the broad shoulders does not scale with the intensity of the narrow peaks, which indicates that these have different origins.

To demonstrate that the narrow peaks in the mass spectra correspond to surface chemical reactions while the broad shoulders correspond to gas-phase chemical reactions, their pump-probe transient evolution is investigated. Figures 4(a) display mass spectra recorded at various pump-probe time delays in the 12.55 μs to 12.90 μs TOF region, which corresponds to I^+. To record the data displayed in Figure 4, CD_3I is continuously dosed on an amorphous cerium oxide surface at a pressure of 2×10^{-8} Torr as measured with the ion gauge detector, while the surface is maintained at 160 K to restrict the amount of CD_3I molecules on the surface to submonolayer.[34] To monitor the transient evolution of the surface and the gas-phase (near-surface) chemical reactions, the surface areas of the narrow peak below 12.6 μs and broad shoulder between 12.62-12.8 μs are plotted as a function of the pump-probe time delay (cf. Figure 4(b)). The pump-probe time dependence of the I^+ narrow peak (black squares in Figure 4(b)) displays the lowest intensity below 100 fs. Subsequently the signal intensity increases, reaches a maximum at 4 ps, and finally decays. This transient signal resembles the unimolecular dissociation dynamics of CD_3I on a cerium oxide surface, obtained by monitoring the I^+ transient signal, which was recently reported by this laboratory.[34] The dashed line in Figure 4(b) is a simulation of the measured I^+ surface transient signal. For the simulation, a model consisting of the delayed

exponential rise and exponential decay functions convoluted with the pump-probe autocorrelation function is employed, in which parameters similar to those obtained in Ref. [34] for the rise (τ_{rise} = 2 ps) and decay (τ_{decay} = 8 ps) time constants of I^+ and the minimum dissociation (t_0=125 fs) of CD_3I on a cerium oxide surface are used. Indeed, this simulation matches well the measured data, which demonstrates that the narrow peak in Figure 4(a) corresponds to atomic iodine obtained through the photoinduced CD_3I dissociation at the surface.

The time dependence of the I^+ broad shoulder (black circles in Figure 4(b)) displays the lowest intensity below 100 fs and a constant high intensity at all other pump-probe time delays measured in this experiment. This transient signal is well reproduced (cf. solid curve in Figure 5(b)) by a model consisting of a delayed step function convoluted with the pump-probe autocorrelation function, in which a coherent delay t_0 of 120 fs[41] is used, representing the gas-phase dissociation time of methyl iodide through the $^3Q_0$ state, which is the strongest optically allowed transition between the ground state and A-band. Indeed, the time dependence of the I^+ broad shoulder in Figure 5(b) resembles the previously reported transient signals obtained during the unimolecular dissociation dynamics of methyl iodide molecule in the gas-phase after the A-band excitation,[25-29] demonstrating that the broad shoulder is due to a gas-phase reaction.

The data presented in Figure 4 clearly demonstrates that the employed experimental method is not only able to distinguish between photoinduced gas-phase and surface chemical reactions at interfaces, but it can also accurately and simultaneously monitor the ultrafast reaction dynamics at the surface and near-surface. Another example that leads to the same conclusion is presented in Section S3 of the Supplementary Material, in which the ultrafast evolution dynamics of the CD_3I sharp peak and broad shoulder (cf. inset in Figure 3) are simultaneously monitored.

B. Confirming the origin of narrow and broad peaks in the mass spectra

To further demonstrate that the narrow peaks in the mass spectra correspond to surface chemical reactions while the broad shoulders correspond to gas-phase chemical reactions, additional investigations are performed. By controlling the gas-phase pressures and surface temperatures experimental conditions can be obtained that facilitate either the adsorption of the molecules on the surface and a negligible density of molecules in the gas-phase or vice versa, i.e., a large density of molecules in gas-phase and a negligible amount on the surface. An example is displayed in Figure S3 in the Supplementary Material.

The result of another experiment that unambiguously demonstrates the origin of the narrow peaks and broad shoulders is displayed in Figure 5. In this experiment, mass spectra are recorded from CH_3I dosed on the surface of a stainless steel repeller plate at different pressures as well as through a hole drilled in the repeller plate while the signal corresponding to CH_3^+ is monitored. The repeller plate is attached to the sample holder, below the sample surface on which all experiments presented in this work are performed (cf. insert in Figure 5).

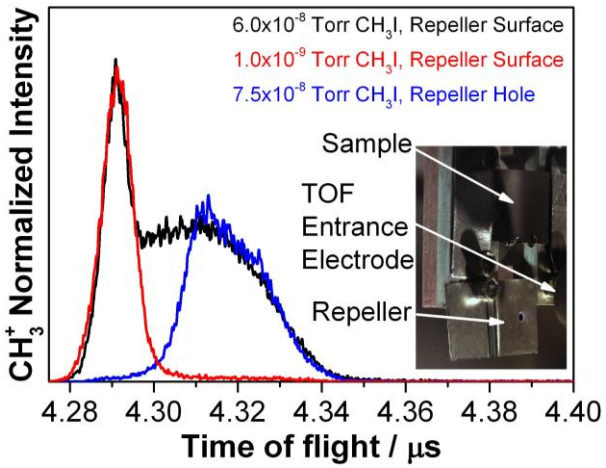

Figure 5. *CH_3^+ region of mass spectra recorded from CH_3I dosed on the surface of a stainless steel repeller held at 100 K at different pressures as well as through a hole drilled in the repeller plate. Insert: Picture showing the repeller plate attached to the sample holder, the sample, and the entrance electrode in the TOF-MS.*

When the repeller is exposed to a CH_3I partial pressure of 8×10^{-8} torr, a significant amount of molecules are adsorbed on the surface and present above the surface, and therefore, a CH_3^+ sharp peak followed by a broader shoulder is observed. When the gas-phase pressure is reduced to $1x10^{-9}$ Torr, molecules are adsorbed on the surface while their concentration above the surface is negligible, which results in a mass spectrum that displays only a sharp peak. When the CH_3I partial pressure above the repeller electrode is high and the

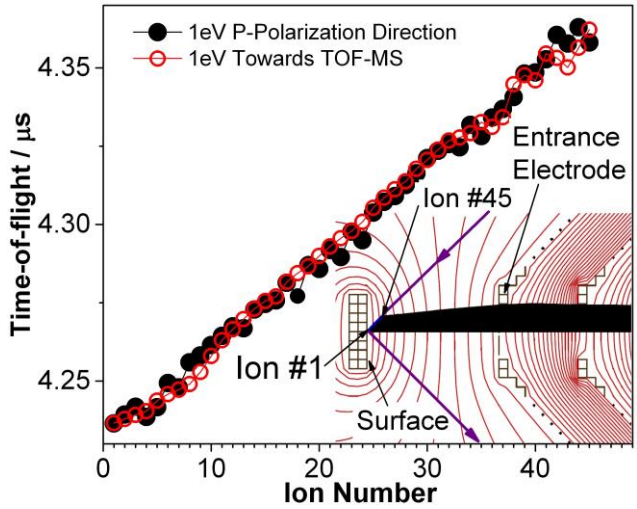

Figure 6. *(a) SimION simulation of the time-of-flight of CH_3^+ formed at the surface and in the gas phase as a function of ions starting point on the incident laser beam path. Inset: SimION simulation displaying the surface, TOF-MS entrance electrode, incident and reflect laser beams, the ion starting points and their trajectories (black curves) as well as the equipotential lines (red curves). See text for details.*

laser light is carefully directed through the hole of the repeller plate, only a broad peak is detected, corresponding to the detection of gas-phase ions.

It needs to be mentioned that sharp peaks followed by broad shoulders were observed in photoinduced interfacial reactions for various combinations of molecules such as CH_3I, CD_3I, CH_3COCH_3, $Fe(CO)_5$, and solid surfaces such as semiconductors, insulators, and metals. This indicates that this technique can be used for a large variety of interfacial photoinduced reactions to simultaneously monitor the ultrafast dynamics at the surface and above the surface. The gas-phase contribution become noticeable at partial pressures of 2×10^{-8} Torr and higher, as measured with the ion gauge detector.

As observed in the mass spectra displayed in this work, the narrow peaks corresponding to surface chemical reactions always appear in the mass spectra in front of the broad shoulders that correspond to gas-phase chemical reactions. This means that ions produced in gas-phase above the surface, which are closer to the TOF-MS, need a longer time-of-flight to be detected than the ions produced at the surface, which are further away from the TOF-MS.

To provide an explanation for the time-of-flight of these ions, SimION simulations[36] are performed in which the trajectories of 45 ions are simulated and the time-of-flight of each ion is plotted as a function of the ion starting point (cf. Figure 6). The first ion (Ion #1 in Figure 6) has a starting point on the surface along the longitudinal axis of the TOF-MS. All the other ions have the starting points on the incident laser beam, each ion being displaced on the horizontal and vertical axis by 0.0375 mm relative to the previous ion. The initial kinetic energy of all ions is 1 eV. Two initial velocities of the ions are considered; one in which the initial velocity of the ions is in the direction of the laser polarization (P-polarization) and one in which the ions are directed toward the spectrometer, with the velocity parallel with the longitudinal axis of the spectrometer. Details on the initial velocities of the ions are presented in Section S5 of the Supplementary Material. As can be seen in Figure 6, the starting direction of the ions has a less significant effect on the time-of-flight than the starting position of the ions. Ion #1, which has the starting point on the surface has the shortest time-of-flight, while all ions originating from the gas-phase have a time-of-flight that gradually increases as their starting position is shifted away from the surface. Ion # 45, which has the starting point nearest to TOF-MS, has the longest time-of-flight. The simulation presented in Figure 6 is in very good agreement with the mass spectra displayed in this study (e.g. Figure 5). It confirms that ions originating on the surface that are further away from the TOF-MS have a shorter time-of-flight than the ions formed in the gas-phase, which are formed closer to the TOF-MS. This is attributed to the inhomogeneous electric field between the surface and entrance electrode of the TOF-MS. The positive ions produced at the surface and above the surface will follow the electric field vectors (not shown), which are perpendicular to the equipotential lines displayed in Figure 6. Therefore, ions formed on the surface are directed along the longitudinal axis of the spectrometer, which is the shortest and the fastest path towards the center of the TOF-MS entrance and detector. Ions formed on the laser path above the surface are directed toward the TOF-MS entrance and detector on a curved trajectory, which requires a longer time-of-flight than the ions formed on the surface.

IV. CONCLUSIONS

This contribution describes an experimental method that can monitor simultaneously the ultrafast dynamics at the surface and near-surface in photoinduced heterogeneous reactions at the solid-gas interface. The method relies on a combination of mass spectrometry and femtosecond pump-probe spectroscopy. As a model system, the ultrafast photoinduced reaction dynamics of methyl iodide at the surface and above the surface of cerium oxide films are investigated. The species that are simultaneously detected from the surface and above the surface present distinct features in the mass spectra, such as a sharp peak followed by an adjacent broad shoulder. The sharp peak is attributed to the species detected from the surface while the broad shoulder is due to the detection of gas-phase species above the surface, as confirmed by several experiments. The evolution of the sharp peak and broad shoulder as a function of the pump-probe time delay resemble transient signals available in the literature that describe the ultrafast reaction dynamics of methyl iodide on a cerium oxide surface[34] and the ultrafast dissociation dynamics of methyl iodide in gas-phase.[25-29] In the end, SimION simulations are performed to understand why the ions produced in the gas-phase, close to the TOF-MS entrance need a longer time-of-flight to reach the TOF-MS detector than the ions produced on the surface which are produced further away from the TOF-MS entrance. The simulations revealed that the difference in the time-of-flight of the ions is due to the inhomogeneous electric field which favors the ions originating on the surface to take the shortest and fastest path toward TOF-MS entrance and spectrometer.

SUPPLEMENTARY MATERIAL

Details of the experimental setup, sample preparation and characterization, SimION simulation, as well as additional mass spectra and pump-probe transient signals are provided in the Supplementary Material.

ACKNOWLEDGMENTS

This material is based upon work supported by the National Science Foundation (NSF) CAREER award CHE-1943697 and the NSF Partnerships for Research and Education in Materials (PREM) Grant DMR-2121953. MEV acknowledges fruitful discussions with Nils Hansen and Jonathan Frank of Sandia National Laboratories. GT acknowledges financial support offered by UCF Office of Undergraduate Research.

AUTHOR DECLARATIONS

Conflict of Interest: The authors have no conflicts to disclose.

Author Contributions

Keith Blackman: Data acquisition (equal); Writing – review & editing (equal); Formal analysis (supporting). **Eric Segrest**: Data acquisition (equal); SimION simulation (supporting); Formal analysis (supporting); Writing – review & editing (equal). **Kai Machamer**: Data acquisition (equal); Writing – review & editing (supporting). **George Turner:** Data acquisition (equal). **Aakash Gupta**: Data acquisition (equal); Writing – review & editing (supporting). **Md. Afjal Khan Pathan**: Data acquisition (equal). **Novia Berriel**: Sample preparation and characterization (equal); Writing – review & editing (equal). **Parag Banarje**: Sample preparation and characterization (lead); Funding acquisition (supporting); Writing – review & editing (equal). **Mihai E. Vaida**: Conceptualization (lead); Data curation (lead); Formal analysis (lead); Funding acquisition (lead); Methodology (lead); SimION simulation (lead); Project administration (lead); Resources (lead); Supervision (lead); Validation (lead); Writing – original draft (lead); Writing – review & editing (lead).

DATA AVAILABILITY

The data that support the findings of this study are available from the corresponding author upon reasonable request.

REFERENCES

1. G. A. Somorjai, H. Frei and J. Y. Park, J. Am. Chem. Soc. **131**, 16589 (2009).
2. F. Gao and D. W. Goodman, Annu. Rev. Phys. Chem. **63**, 265 (2012).
3. M. A. Bañares, M. O. Guerrero-Pérez, J. L. G. Fierro and G. G. Cortez, Journal of Materials Chemistry **12**, 3337 (2002).
4. B. M. Weckhuysen, Chem. Commun. (Cambridge, U. K.)97 (2002).
5. M. A. Bañares and I. E. Wachs, J. Raman Spectrosc. **33**, 359 (2002).
6. G. G. Cortez and M. A. Bañares, J. Catal. **209**, 197 (2002).
7. B. Zhou, E. Huang, R. Almeida, S. Gurses, A. Ungar, J. Zetterberg, A. Kulkarni, C. X. Kronawitter, D. L. Osborn, N. Hansen and J. H. Frank, ACS Catalysis **11**, 155 (2021).
8. A. H. Zewail, Science **242**, 1645 (1988).
9. M. E. Vaida and T. M. Bernhardt, Rev. Sci. Instrum. **81**, 104103 (2010).
10. S. J. Riley and K. R. Wilson, Faraday Discuss. Chem. Soc. **53**, 132 (1972).
11. R. K. Sparks, K. Shobatake, L. R. Carlson and Y. T. Lee, J. Chem. Phys. **75**, 3838 (1981).
12. D. W. Chandler, J. W. Thoman, M. H. M. Janssen and D. H. Parker, Chemical Physics Letters **156**, 151 (1989).
13. R. A. Hertz and J. A. Syage, J. Chem. Phys. **100**, 9265 (1994).
14. G. Li, H. J. Hwang and H. C. Jung, Rev. Sci. Instrum. **76**, 023105 (2005).
15. G. Li and H. J. Hwang, J. Chem. Phys. **124**, 244306 (2006).
16. L. R. Khundkar and A. H. Zewail, Chemical Physics Letters **142**, 426 (1987).
17. M. Shapiro and R. Bersohn, J. Chem. Phys. **73**, 3810 (1980).
18. Y. Amatatsu, K. Morokuma and S. Yabushita, J. Chem. Phys. **94**, 4858 (1991).
19. B. R. Johnson, J. L. Kinsey and M. Shapiro, J. Chem. Phys. **88**, 3147 (1988).
20. S. Y. Lee and E. J. Heller, J. Chem. Phys. **76**, 3035 (1982).
21. H. Guo, K. Q. Lao, G. C. Schatz and A. D. Hammerich, J. Chem. Phys. **94**, 6562 (1991).
22. H. Guo and G. C. Schatz, J. Chem. Phys. **93**, 393 (1990).
23. A. B. Alekseyev, H.-P. Liebermann, R. J. Buenker and S. N. Yurchenko, J. Chem. Phys. **126**, 234102 (2007).
24. A. B. Alekseyev, H.-P. Liebermann and R. J. Buenker, J. Chem. Phys. **126**, 234103 (2007).
25. P. Y. Cheng, D. Zhong and A. H. Zewail, J. Chem. Phys. **105**, 6216 (1996).
26. D. Zhong and A. H. Zewail, J. Phys. Chem. A **102**, 4031 (1998).
27. R. de Nalda, J. Dura, A. Garcia-Vela, J. G. Izquierdo, J. Gonzalez-Vazquez and L. Banares, J. Chem. Phys. **128**, 244309 (2008).
28. A. García-Vela, R. d. Nalda, J. Durá, J. González-Vázquez and L. Bañares, J. Chem. Phys. **135**, 154306 (2011).
29. M. L. Murillo-Sánchez, J. González-Vázquez, M. E. Corrales, R. d. Nalda, E. Martínez-Núñez, A. García-Vela and L. Bañares, J. Chem. Phys. **152**, 014304 (2020).
30. M. E. Vaida, P. E. Hindelang and T. M. Bernhardt, J. Chem. Phys. **129**, 011105 (2008).
31. M. E. Vaida and T. M. Bernhardt, ChemPhysChem **11**, 804 (2010).
32. M. E. Vaida and T. M. Bernhardt, in *Ultrafast Phenomena in Molecular Sciences: Femtosecond Physics and Chemistry*, edited by R. de Nalda and L. Bañares (Springer International Publishing, Cham, 2014), pp. 231.
33. M. E. Vaida, R. Tchitnga and T. M. Bernhardt, Beilstein J. Nanotechnol. **2**, 618 (2011).
34. M. A. K. Pathan, A. Gupta and M. E. Vaida, J. Phys. Chem. Lett. **13**, 9759 (2022).
35. W. C. Wiley and I. H. McLaren, Rev. Sci. Instrum. **26**, 1150 (1955).
36. D. A. Dahl, International Journal of Mass Spectrometry **200**, 3 (2000).
37. M. A. K. Pathan, A. Gupta and M. E. Vaida, Nanotechnology **32**, 505605 (2021).
38. B. T. Young, M. A. K. Pathan, T. Jiang, D. Le, N. Marrow, T. Nguyen, C. E. Jordan, T. S. Rahman, D. M. Popolan-Vaida and M. E. Vaida, J. Chem. Phys. **152**, 074706 (2020).

39. M. E. Vaida and T. M. Bernhardt, European Physical Journal D: Atomic, Molecular and Optical Physics **52**, 119 (2009).
40. M. E. Vaida, T. B. Rawal, T. M. Bernhardt, B. M. Marsh, T. S. Rahman and S. R. Leone, J. Phys. Chem. Lett. **13**, 4747 (2022).
41. R. de Nalda, J. G. Izquierdo, J. Dura and L. Banares, J. Chem. Phys. **126**, 021101 (2007).